



PF-04859989 as a template for structure-based drug design: Identification of new pyrazole series of irreversible KAT II inhibitors with improved lipophilic efficiency

Amy B. Dounay^{*,†}, Marie Anderson, Bruce M. Bechle, Edelweiss Evrard, Xinmin Gan, Ji-Young Kim, Laura A. McAllister, Jayvardhan Pandit, SuoBao Rong, Michelle A. Salafia, Jamison B. Tuttle, Laura E. Zawadzke, Patrick R. Verhoest

Pfizer Worldwide Research and Development, Neuroscience Medicinal Chemistry, Groton Laboratories, Eastern Point Road, Groton, CT 06340, United States

ARTICLE INFO

Article history:

Received 7 January 2013
Accepted 7 February 2013
Available online 15 February 2013

Keywords:

Kynurenine pathway
Kynurenic acid
Kynurenine aminotransferase
Irreversible inhibitor
Mechanism-based inactivator
Lipophilic efficiency
Schizophrenia

ABSTRACT

The structure-based design, synthesis, and biological evaluation of a new pyrazole series of irreversible KAT II inhibitors are described herein. The modification of the inhibitor scaffold of **1** and **2** from a dihydroquinolinone core to a tetrahydropyrazolopyridinone core led to discovery of a new series of potent KAT II inhibitors with excellent physicochemical properties. Compound **20** is the most potent and lipophilically efficient of these new pyrazole analogs, with a k_{inact}/K_i value of $112,000 \text{ M}^{-1} \text{ s}^{-1}$ and lipophilic efficiency (LipE) of 8.53. The X-ray crystal structure of **20** with KAT II demonstrates key features that contribute to this remarkable potency and binding efficiency.

© 2013 Elsevier Ltd. All rights reserved.

The kynurenine pathway has been implicated in the pathophysiology of a number of psychiatric and neurological disorders, including schizophrenia and bipolar disorder.^{1–3} Initial interest in pharmacological modulation of the kynurenine pathway was prompted, in part, by reports that kynurenic acid (KYNA) antagonizes both the α_7 nicotinic acetylcholine receptor⁴ and the *N*-methyl-D-aspartate (NMDA) receptor.⁵ More recently, KYNA has also been identified as the only known native agonist of the aryl hydrocarbon receptor (AHR).⁶ Elevated KYNA levels have been detected in the cerebrospinal fluid in small cohorts of schizophrenia^{7,8} and bipolar patients,⁹ as well as in the postmortem prefrontal cortex of schizophrenia patients.¹⁰ Thus, reduction of central KYNA levels via modulation of the kynurenine pathway may provide a new therapeutic approach for schizophrenia and other diseases of the central nervous system.

Inhibition of kynurenine aminotransferase (KAT) II, one of several enzymes in the kynurenine pathway, provides a novel mechanism for reduction of KYNA levels in the brain.^{11,12} A number of new KAT II inhibitors have been utilized as pharmacological tools

for preclinical exploration of this mechanism. For example, (*S*)-ESBA and BFF-122 have been investigated as centrally-administered tool compounds.^{13,14} Our team recently reported the discovery of PF-04859989 (**1**), a potent, brain-penetrant inhibitor of KAT II with in vivo activity.¹⁵ The X-ray crystal structure and ¹³C NMR studies of **1** bound to KAT II have demonstrated that this compound forms a covalent adduct with the cofactor, pyridoxal phosphate (PLP), in the enzyme active site. This covalent interaction irreversibly inhibits the enzyme, but without formation of a covalent bond to the protein, thus alleviating the risk of hapten-mediated immunotoxicity. Our preliminary structure–activity relationship (SAR) studies on this scaffold have also shown that substituents at the C6 and C7 positions provide the best opportunities for improved potency. In a recent follow-up report, we have demonstrated that compound **2**, a 6-benzyl-7-methoxy-substituted analog of **1**, is significantly more potent (k_{inact}/K_i) than the parent compound.¹⁶

The key binding features of compound **2** that account for its remarkable KAT II potency are illustrated in Figure 2.¹⁷ Compound **2**, like compound **1**, employs its primary amine functionality in a covalent enamine linkage with PLP, which is bound to KAT II via a network of non-covalent interactions. Additionally, the hydroxamate functionality of **2** engages Arg399 and Asn202 in critical hydrogen-bonding interactions. Compound **2** also gains binding

* Corresponding author. Tel.: +1 719 389 6438; fax: +1 719 389 6182.

E-mail address: amy.dounay@coloradocollege.edu (A.B. Dounay).

† Present address: The Colorado College, Department of Chemistry and Biochemistry, 14 East Cache La Poudre, Colorado Springs, CO 80903, United States.

affinity from van der Waals interactions between the C6-benzyl group and hydrophobic residues, including Leu293, in the 'lipophilic pocket' of KAT II. Unique interactions between KAT II and **2** that further enhance this inhibitor's potency include an apparent cation- π interaction between the aromatic ring of the C6-benzyl group and Arg20, which is further stabilized by a hydrogen bond between Arg20 and the C7-methoxy oxygen. Unfortunately, in vivo efficacy studies of **2** were hampered by rapid clearance of this compound. Although O-glucuronidation is a primary clearance mechanism for all compounds in this series, the more lipophilic compounds, such as **2**, are also susceptible to cytochrome P450 (CYP)-mediated metabolism, resulting in high drug clearance and low exposure.

In order to enable exploration of analogs similar to **2** in which lipophilic phenyl or benzyl substituents are utilized for significant potency gains, our goal was to identify a modified core structure with reduced lipophilicity. A pyrazolopyridinone ring system was envisioned as a viable alternative to the quinolinone core of **1** and **2** (Fig. 1). This new scaffold would afford a drug with more favorable overall physicochemical properties, and preliminary modeling suggested that benzyl or phenyl substituents on the pyrazole ring (R^1 or R^2) could access the lipophilic pocket of KAT II. Appropriately substituted pyrazole analogs might also be able to replicate the unique bidentate interaction of **2** with Arg20 that contributes to the remarkable potency of this compound.

Pyrazole analogs **10–12** were synthesized according to the general route shown in Scheme 1.¹⁸ This synthetic sequence began with the appropriately substituted methoxymethylidene malononitrile **3**, which was condensed with methylhydrazine in ethanol under reflux to afford the corresponding 5-amino-1-methyl-1H-pyrazole-4-carbonitrile **4**. Nitrile hydrolysis followed by oxidation of the 5-amino group yielded nitropyrazole **6**. Reduction of the carboxylic acid using borane-dimethylsulfide provided a primary alcohol, which was converted to bromide **7** using carbon tetrabromide and triphenylphosphine. Asymmetric alkylation of **7** was accomplished using phase-transfer-catalyzed alkylation with a glycinate Schiff base to afford **8** with high enantioselectivity.^{19,20} Activation of the carboxylic acid functionality as the trifluoroethyl ester was critical to the success of the reductive cyclization in this series.^{20,21} Thus, global deprotection of **8** using TFA was followed by protection of the amine functionality as its Boc derivative. Subsequent activation of the carboxylic acid via esterification with 2,2,2-trifluoroethanol provided **9**. Finally, reductive cyclization using platinum on carbon in pyridine was followed by deprotection of the Boc group to give pyrazole analogs **10–12**.

The synthesis of pyrazole analogs **19** and **20** was completed using an analogous route, as shown in Scheme 2. To achieve this substitution pattern on the pyrazole core, the general method of Xia and co-workers was applied.²² The desired regioselectivity was achieved by condensation of the appropriately activated methyldiene malononitrile or analogous ethyl cyanoacetate deriv-

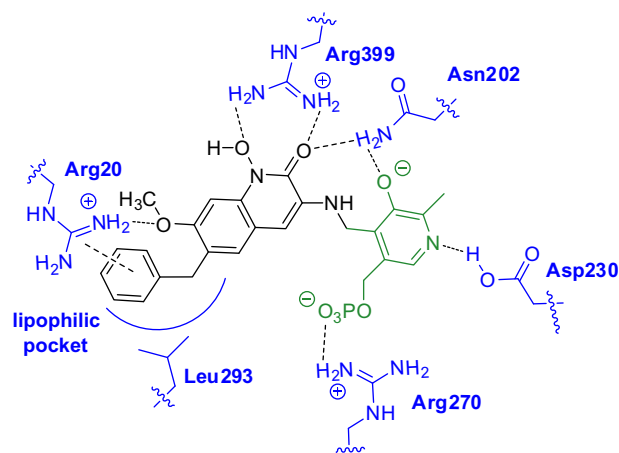


Figure 2. Key interactions of the 2-PLP adduct in the KAT II active site.

ative (**13**) with a benzaldehyde hydrazone (**14**). Oxidation of the amino group was accomplished using sodium perborate tetrahydrate in trifluoroacetic acid, and subsequent ester hydrolysis yielded carboxylic acid **16**. The conversion of **16** to pyrazole analogs **19** and **20** used the same general route and methods described in Scheme 1 for analogs **10–12**.

New pyrazole analogs were initially assessed for IC_{50} in our KAT II screening assay.¹⁵ The IC_{50} values were used in a primary triage step to discriminate between 'actives' and 'inactives'. Compounds with $IC_{50} \leq 100$ nM were advanced to the k_{inact}/K_i assay, which was used for more rigorous evaluation of the SAR in the series (Table 1). Pyrazole **10** was prepared as an unadorned analog of **1** to preliminarily assess the compatibility of the pyrazole scaffold with KAT II. Capping of the pyrazole with a methyl substituent avoids the introduction of an additional hydrogen-bond donor, thereby keeping the overall physicochemical properties in reasonable space for CNS-penetrant compounds.²³ Pyrazole **10** showed moderate potency (329 nM) in the preliminary KAT II assay, suggesting that further follow-up on this scaffold was warranted. The methyl substituent in **10** was actually better tolerated than in the analogous C8-methyl analog of **1** (1050 nM),¹⁵ suggesting that maintaining this *N*-methyl group could be feasible as the substitution pattern on the scaffold was further optimized. Our previous structure-based drug design around compound **2** had demonstrated that significant potency gains were achieved by appending the C6-benzyl group. To test the translatability of this finding to the pyrazole series, pyrazole **11** was prepared and evaluated. Once again, the benzyl substitution provided a significant improvement in potency (64 nM), and the k_{inact}/K_i for compound **11** ($16,000 \text{ M}^{-1} \text{ s}^{-1}$) was comparable to that of our initial lead compound **1** ($18,500 \text{ M}^{-1} \text{ s}^{-1}$). In the previous series, additional modest

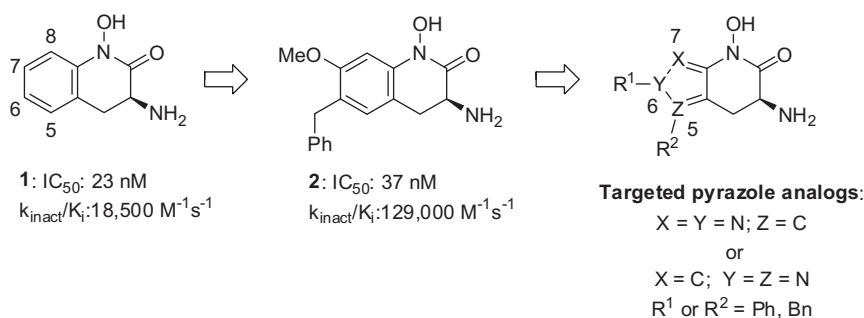
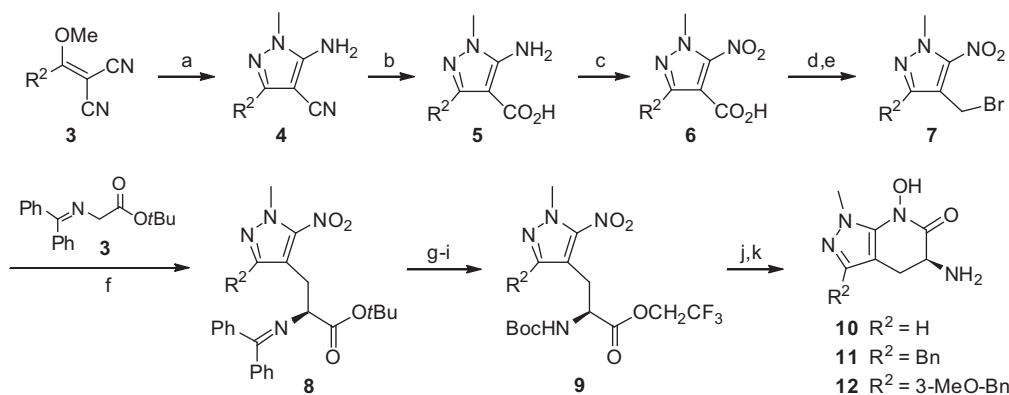
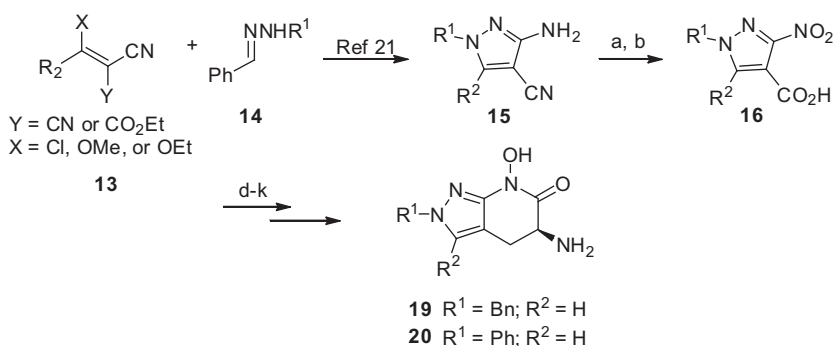


Figure 1. Design of new pyrazole series based on KAT II inhibitors **1** and **2**.



Scheme 1. Synthesis of compounds **10–12**. Reagents and conditions: (a) methylhydrazine, ethanol, reflux; (b) NaOH (aq), reflux; (c) NaNO₂, HBF₄ (aq); Cu/NaNO₂; (d) BH₃-DMS, THF, –20 °C to reflux; (e) CBr₄, PPh₃, CH₂Cl₂; (f) *O*-allyl-*N*-(9-anthracenylmethyl)cinchonidinium bromide, CsOH·H₂O, CH₂Cl₂, –30 °C; (g) TFA, CH₂Cl₂; (h) Boc₂O, NaOH, THF; (i) 1-[3-(dimethylamino)propyl]-3-ethylcarbodiimide hydrochloride, DMAP, 2,2,2-trifluoroethanol, CH₂Cl₂; (j) 5% Pt/C, H₂ (30 psi), pyridine; (k) HCl, dioxane.



Scheme 2. General synthetic approach toward pyrazole analogs **19–20**. Reagents and conditions (a) sodium perborate tetrahydrate, TFA; (b) LiOH (aq.), MeOH; (d–k): see Scheme 1.

potency gains were achieved with substituents on the benzyl group, but the same trends were not observed in the pyrazole series (e.g., compound **12**, Table 1).

An isomeric pyrazole scaffold (compounds **17**²⁴ and **18**,²⁵ Table 1) was also explored. This structural variation was designed to project the benzyl substituent into the lipophilic pocket of KAT II, in analogy to analogs **2** and **11**, without requiring the *N*-methyl group to cap the 1*H*-pyrazole. Although the trifluoromethyl group of **17** was tolerated, pyrazole **18**, which is unsubstituted at the 7 position, achieved comparable potency to **11** while providing slightly improved ligand efficiency.

The phenyl group was next examined on the 6-position of the pyrazole scaffold. In the expectation that this substitution pattern would continue to project the phenyl into the lipophilic pocket of KAT II, pyrazoles **19–21** were prepared and evaluated (Table 1). Pyrazole **19**, which is isomeric with pyrazole **18**, showed a slight loss in potency (10,500 M^{–1} s^{–1}) relative to **18** (16,200 M^{–1} s^{–1}). Remarkably, the *N*-Ph pyrazole **20**, which differs from **19** only in the deletion of one methylene group, provided a dramatic improvement in k_{inact}/K_i (112,000 M^{–1} s^{–1}). Pyrazole **20** thus emerged as one of our most potent KAT II inhibitors discovered to date, approaching the potency of compound **2**. The subtlety of the SAR in this series is further highlighted by pyrazole **21**,²⁶ which is isomeric with **20**, but is significantly less potent in the k_{inact}/K_i assay (8580 M^{–1} s^{–1}). Pyrazoles **20** and **21** confirm that the pyrazole core not only serves as a scaffold to project the phenyl substituent into an optimal position in the lipophilic pocket, but that the atoms in the pyrazole ring can also provide either favorable or unfavorable interactions with KAT II.

The X-ray crystal structure of pyrazole **20** with KAT II provides useful insights into the unique potency of this inhibitor (Fig. 3). Like all of our active irreversible inhibitors, the primary amine of **20** reacts with the aldehyde functionality of PLP in the active site of KAT II to form an enamine adduct.¹⁵ Likewise, as in our previous X-ray structures of KAT II inhibitors, the hydroxamate functional group is involved in a number of hydrogen bonding interactions with Arg399 and Asn202. Our selection of the *N*-phenyl group to optimize lipophilic interactions plays out well with **20**, in which the phenyl group interacts with multiple hydrophobic residues that line the entrance tunnel to the substrate-binding site, including Ile19, Leu40, and Tyr74. Although the phenyl group of **20** does not appear to form a cation– π interaction with Arg20 as was observed in the X-ray structure of **2**, the domain consisting of Ile19 to Gly29 of KAT II forms an ordered α -helical structure, a feature that has generally been observed in co-structures of KAT II with our most potent inhibitors.¹⁶ The X-ray structure of **20** also provides an explanation for the dramatic potency difference between **20** and the isomeric pyrazole analog **21**. The N7-nitrogen atom of **20** (see Fig. 1) is appropriately positioned (3.0 Å) to interact with a water molecule in the active site, thereby further enhancing the potency of this inhibitor. Likewise, the unsubstituted C5 carbon of the pyrazole ring is well accommodated in the lipophilic pocket bounded by Tyr 74. In contrast, the isomeric pyrazole **21** cannot take advantage of a similar water molecule interaction. Furthermore, pyrazole **21** projects its nitrogen atom at position 5 (see Fig. 1) into the lipophilic pocket bounded by Tyr74. Thus, pyrazole **21** is doubly penalized for this reversal of polarity in its pyrazole scaffold.

Table 1
Selected data for KAT II inhibitors

Compound	Structure	hKAT II ^a IC ₅₀ (nM)	k_{inact}/K_i^b (M ⁻¹ s ⁻¹)	k_{inact}^b (min ⁻¹)	K_i^a (nM)	cSF log D ^c	LipE ^d
1 (PF-04859989)		23	18,500	0.0156	14	0.079	7.77
2		37	129,000	0.0146	1.6	2.07	6.73
10		329	ND	ND	ND	-0.67	ND
11		64	16,000	0.0349	32	0.29	7.20
12		66	8710	0.0116	22	0.61	7.04
17		74	7920	0.0227	48	1.17	6.15
18		23	16,200	0.0116	12	0.22	7.70
19		47	10,500	0.0147	23	0.16	7.48
20		25	112,000	0.0125	1.9	0.20	8.53
21		85	8580	0.0144	41	0.37	6.99

^a Values are geometric means of two or more experiments conducted in duplicate. See Ref. 15 for detailed assay protocols.

^b Values are arithmetic of two or more experiments conducted in duplicate.

^c Calculated shake flask (SF) distribution coefficient at pH 7.4.

^d Calculated LipE = $-\log(K_i) - \text{cSF log } D$.

Further evaluation of the k_{inact}/K_i data set provides additional insights on this novel pyrazole series of KAT II inhibitors. Our previous evaluation of k_{inact}/K_i trends for inhibitors **1** and **2** and their analogs showed that the potency differences among analogs were

largely driven by differences in the K_i term, which describes the non-covalent binding affinity; the k_{inact} term, which describes the rate of covalent bond formation, remained relatively constant across compounds in the series.^{15,16} The same trend is observed

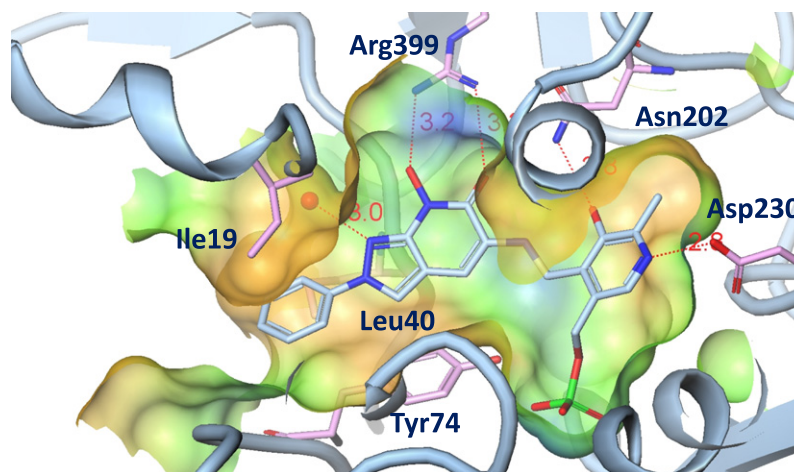


Figure 3. X-ray structure of adduct formed by **20** with PLP in the KAT II active site. The surface is colored by increasing hydrophobicity, from blue to green to brown.

for the new series of pyrazole analogs (Table 1). The most potent new analog, pyrazole **20**, has a K_i of 1.9 nM, which is comparable to the K_i of compound **2** (1.6 nM), our most potent analog from the original series.

In order to evaluate progress against our original goal of identifying a less lipophilic core structure for elaboration to potent KAT II inhibitors, the lipophilicity of these analogs was assessed using calculated shake flask $\log D$ (cSF $\log D$) values (Table 1).^{27,28} This lipophilicity term was used in conjunction with the potency term K_i to calculate lipophilic ligand efficiency (LipE), a parameter that normalizes potency differences relative to a compound's lipophilicity, allowing for a direct comparison between compounds.²⁹ A comparison of the LipE of our new pyrazole analogs demonstrates that these compounds generally achieve comparable lipophilic efficiency to lead compound **1** and improved efficiency relative to compound **2** (Table 1). Notably, pyrazole **20** shows significantly improved LipE (8.53) over compounds **1** (7.77) and **2** (6.73) and emerges as our most efficient KAT II inhibitor identified to date. As anticipated, the lower $\log D$ of **20** relative to **2** also results in reduction of CYP-mediated clearance. The measured clearance (intrinsic, apparent) in a human liver microsome assay³⁰ improved from 26.0 $\mu\text{L}/\text{min}/\text{mg}$ for compound **2** to <8.0 $\mu\text{L}/\text{min}/\text{mg}$ for compound **20**.

In summary, our structure-based drug design approach has enabled the identification of a new pyrazole series of irreversible KAT II inhibitors. Optimization within this new series led to the discovery of **20**, which displays significantly improved LipE and provides a new template for further preclinical investigation of KAT II as a novel mechanism for treatment of CNS disorders.

Acknowledgment

We would like to thank Brian Campbell, Christine Strick, and Scot Mente for helpful discussions and Katherine Brightly for careful editing of this manuscript.

Supplementary data

Supplementary data associated with this article can be found, in the online version, at <http://dx.doi.org/10.1016/j.bmcl.2013.02.039>.

References and notes

- Erhardt, S.; Schwieler, L.; Nilsson, L.; Linderholm, K.; Engberg, G. *Physiol. Behav.* **2007**, *92*, 203.
- Erhardt, S.; Olsson, S. K.; Engberg, G. *CNS Drugs* **2009**, *23*, 91.
- Potter, M. C.; Elmer, G. I.; Bergeron, R.; Albuquerque, E.; Guidetti, P.; Wu, H.-Q.; Schwarcz, R. *Neuropsychopharmacology* **2010**, *35*, 1734.
- Hilmas, C.; Pereira, E. F.; Alkondon, M.; Rassoulpour, A.; Schwarcz, R.; Albuquerque, E. X. *J. Neurosci.* **2001**, *21*, 7463.
- Kessler, M.; Terramani, T.; Lynch, G.; Baudry, M. *J. Neurochem.* **1989**, *52*, 1319.
- Natale, B. C.; Murray, I. A.; Schroeder, J. C.; Flaveny, C. A.; Lahoti, T. S.; Laurenzana, E. M.; Omiecinski, C. J.; Perdue, G. H. *Toxicol. Sci.* **2010**, *115*, 89.
- Erhardt, S.; Blennow, K.; Nordin, C.; Skogh, E.; Lindstrom, L. H.; Engberg, G. *Neurosci. Lett.* **2001**, *313*, 96.
- Nilsson, L. K.; Linderholm, K. R.; Engberg, G.; Paulson, L.; Blennow, K.; Lindstrom, L. H.; Nordin, C.; Karanti, A.; Persson, P.; Erhardt, S. *Schizophr. Res.* **2005**, *80*, 315.
- Olsson, S. K.; Samuelsson, M.; Saetre, P.; Lindstrom, L.; Jonsson, E. G.; Nordin, C.; Engberg, G.; Erhardt, S.; Landen, M. *J. Psychiatry Neurosci.* **2010**, *35*, 195.
- Schwarcz, R.; Rassoulpour, A.; Wu, H.-Q.; Medoff, D.; Tamminga, C. A.; Roberts, R. C. *Biol. Psychiatry* **2001**, *50*, 521.
- Han, Q.; Cai, T.; Tagle, D. A.; Li, J. *Cell. Mol. Life Sci.* **2010**, *67*, 353.
- Rossi, F.; Garavaglia, S.; Montalbano, V.; Walsh, M. A.; Rizzi, M. *J. Biol. Chem.* **2008**, *283*, 3559.
- Rossi, F.; Valentina, C.; Garavaglia, S.; Sathyaikumar, K. V.; Schwarz, R.; Kojima, S.; Okuwaki, K.; Ono, S.; Kajii, Y.; Rizzi, M. *J. Med. Chem.* **2010**, *53*, 5684.
- Pellicciari, R.; Rizzo, R. C.; Costantino, G.; Marinuzzi, M.; Amori, L.; Guidetti, P.; Wu, H.-Q.; Schwarcz, R. *ChemMedChem* **2006**, *1*, 528.
- Dounay, A. B.; Anderson, M.; Bechle, B. M.; Campbell, B. M.; Claffey, M. M.; Evdokimov, A.; Evrard, E.; Fonseca, K. R.; Gan, X.; Ghosh, S.; Hayward, M. M.; Horner, W.; Kim, J.-Y.; McAllister, L. A.; Pandit, J.; Paradis, V.; Parikh, V. D.; Reese, M. R.; Rong, S.; Salafia, M. A.; Schuyten, K.; Strick, C. A.; Tuttle, J. B.; Valentine, J.; Wang, H.; Zawadzke, L. E.; Verhoest, P. R. *ACS Med. Chem. Lett.* **2012**, *3*, 187.
- Tuttle, J. B.; Anderson, M.; Bechle, B. M.; Campbell, B. M.; Chang, C.; Dounay, A. B.; Evrard, E.; Fonseca, K. R.; Gan, X.; Ghosh, S.; Horner, W.; James, L. C.; Kim, J.-Y.; McAllister, L. A.; Pandit, J.; Parikh, V. D.; Rago, B. J.; Salafia, M. A.; Strick, C. A.; Zawadzke, L. E.; Verhoest, P. R. *ACS Med. Chem. Lett.* **2013**, *4*, 37.
- For X-ray structure of **2** bound to KAT II, see Ref. 16.
- Full experimental details are contained within the following patent application: Dounay, A. B.; McAllister, L. A.; Parikh, V. D.; Rong, S.; Verhoest, P. R. *PCT Int. Appl.* **2012**, WO 2012073143.
- Corey, E. J.; Noe, M. C.; Xu, F. *Tetrahedron Lett.* **1998**, *39*, 5347.
- McAllister, L. A.; Bechle, B. M.; Dounay, A. B.; Evrard, E.; Gan, X.; Ghosh, S.; Kim, J.-Y.; Parikh, V. D.; Tuttle, J. B.; Verhoest, P. R. *J. Org. Chem.* **2011**, *76*, 3484.
- The ester activation step was necessary to prevent over-reduction to a lactam by-product under the reductive cyclization conditions.
- Xia, Y.; Chackalamannil, S.; Czarniecki, M.; Tsai, H.; Vaccaro, H.; Cleven, R.; Cook, J.; Fawzi, A.; Watkins, R.; Zhang, H. *J. Med. Chem.* **1997**, *40*, 4372.
- Wager, T. T.; Villalobos, A.; Verhoest, P. R.; Hou, X.; Shaffer, C. L. *Expert Opin. Drug Discov.* **2011**, *6*, 371.
- Prepared in analogy to compound **18**, starting from 3-methyl-5-(trifluoromethyl)-1H-pyrazole as described by Acker, B. A.; Hughes, R. O.; Jacobsen, E. J.; Lu, H.-F.; Rogers, T. E.; Tollefson, M. B.; Walker, J. K. *PCT Int. Appl.* **2006**, WO 2006046135.
- Prepared from methyl 1-benzyl-4-nitro-1H-pyrazole-5-carboxylate using the general methods described in Schemes 1 and 2. Commercially available 4-nitro-1H-pyrazole-3-carboxylic acid was converted to 1-benzyl-4-nitro-1H-pyrazole-5-carboxylate over two steps.
- Pyrazole **21** was prepared following the general route shown in Scheme 1. In this case, arylation of methyl 4-nitro-1H-pyrazole-3-carboxylate followed by ester hydrolysis provides 4-nitro-1-phenyl-1H-pyrazole-3-carboxylic acid, following the method of Miller, T. A. Sloman, D. L.; Stanton, M. G.; Wilson, K. J.; Witter, D. J. *PCT Int. Appl.* **2007**, WO 2007087129. Subsequent conversion of the carboxylic acid moiety to a primary bromide may be effected as described

- in Scheme 1. The resulting 3-(bromomethyl)-4-nitro-1-phenyl-1*H*-pyrazole was converted to 3-(4-nitro-1-phenyl-1*H*-pyrazol-3-yl)alanine using chemistry reported by Crestey, F.; Collot, V.; Stiebing, S.; Rault, S. *Tetrahedron* **2006**, *62*, 7772.
27. For a description of the use of SF log*D* and other ADME data sets in a prospective manner, see Keefer, C. E.; Chang, G.; Kauffman, G. W. *Bioorg. Med. Chem.* **2011**, *19*, 3739.
28. The experimental shake-flask log*D* values for compounds in this series have shown excellent correlation with in silico SF log*D* values calculated with our new model (Christopher Keefer, Pfizer, unpublished results.)
29. Edwards, M. P.; Price, D. A. *Annu. Rep. Med. Chem.* **2010**, *45*, 381.
30. Hop, C. E.; Cole, M. J.; Davidson, R. E.; Duignan, D. B.; Federico, J.; Janiszewski, J. S.; Jenkins, K.; Krueger, S.; Lebowitz, R.; Liston, T. E.; Mitchell, W.; Snyder, M.; Steyn, S. J.; Soglia, J. R.; Taylor, C.; Troutman, M. D.; Umland, J.; West, M.; Whalen, K. M.; Zelesky, V.; Zhao, S. X. *Curr. Drug Metab.* **2008**, *9*, 847.